Microsc. Microanal. 15, 338–344, 2009
doi:10.1017/S1431927609090813

Microscopy AND Microanalysis

Nuclear Microscopy: A Novel Technique for Quantitative Imaging of Gadolinium Distribution within Tissue Sections

Reshmi Rajendran,[1,*,†] John A. Ronald,[2,†] Tao Ye,[1] Ren Minqin,[1] John W. Chen,[3] Ralph Weissleder,[3] Brian K. Rutt,[2] Barry Halliwell,[4] and Frank Watt[1]

[1]*Centre for Ion Beam Applications, Department of Physics, National University of Singapore, Singapore*
[2]*Robarts Research Institute, University of Western Ontario, London, Ontario, Canada*
[3]*Center for Molecular Imaging Research, Department of Radiology, Massachusetts General Hospital, Boston, MA, USA*
[4]*Department of Biochemistry, National University of Singapore, Singapore*

Abstract: All clinically-approved and many novel gadolinium (Gd)-based contrast agents used to enhance signal intensity in magnetic resonance imaging (MRI) are optically silent. To verify MRI results, a "gold standard" that can map and quantify Gd down to the parts per million (ppm) levels is required. Nuclear microscopy is a relatively new technique that has this capability and is composed of a combination of three ion beam techniques: scanning transmission ion microscopy, Rutherford backscattering spectrometry, and particle induced X-ray emission used in conjunction with a high energy proton microprobe. In this proof-of-concept study, we show that in diseased aortic vessel walls obtained at 2 and 4 h after intravenous injection of the myeloperoxidase-senstitive MRI agent, bis-5-hydroxytryptamide-diethylenetriamine-pentaacetate gadolinium, there was a time-dependant Gd clearance (2 h = 18.86 ppm, 4 h = 8.65 ppm). As expected, the control animal, injected with the clinically-approved conventional agent diethylenetriamine-pentaacetate gadolinium and sacrificed 1 week after injection, revealed no significant residual Gd in the tissue. Similar to known *in vivo* Gd pharmacokinetics, we found that Gd concentration dropped by a factor of 2 in vessel wall tissue in 1.64 h. Further high-resolution studies revealed that Gd was relatively uniformly distributed, consistent with random agent diffusion. We conclude that nuclear microscopy is potentially very useful for validation studies involving Gd-based magnetic resonance contrast agents.

Key words: gadolinium, magnetic resonance imaging, nuclear microscopy, PIXE, STIM, RBS, atherosclerosis

Introduction

Magnetic resonance imaging (MRI) is a powerful noninvasive, nonionizing imaging modality that is primarily used for medical imaging but also plays an important role in basic science research. It can provide anatomical, functional, metabolic, cellular, and molecular information of tissues *in vivo* with high resolutions in three dimensions, routinely down to 1 mm at clinical field strengths and even down to about 50 μm in research settings (Strijkers et al., 2007). Soft tissue contrast in magnetic resonance images is generated by highlighting differences in the longitudinal (T_1) and transverse (T_2) relaxation times of protons in different tissues. Tissue differences can be made greater by shortening T_1 and/or T_2; shortening of T_1 is often preferred as this leads to gain of signal versus loss of signal via shortening of T_2.

To shorten either T_1 or T_2, contrast agents (CAs), which are diagnostic pharmaceutical compounds containing paramagnetic or superparamagnetic metal ions (Bellin, 2006), are administered. The influence of a paramagnetic ion on the relaxation time depends directly upon the number of unpaired electrons generating the electronic spin that interferes with the nuclear spin of hydrogen (Idee et al., 2006). Gd (III) ions, which are paramagnetic, contain seven unpaired electrons and yield very strong T_1 relaxation properties (Brasch, 1992); making Gd compounds the most widely used CAs in MRI. For Gd to be safely administered *in vivo*, a chelator such as diethylene triamine pentaacetic acid (DTPA) that prevents Gd toxicity must be used.

Aim

To verify the *in vivo* imaging results obtained using Gd-chelates in MRI, a complementary technique is required to map Gd spatially and simultaneously quantify Gd down to

Received January 23, 2009; accepted June 2, 2009
*Corresponding author. E-mail: reshmi_rajendran@sbic.a-star.edu.sg
†R.R. and J.A.R. contributed equally to this work.

the parts per million (ppm) level and normalized to the density of the tissue. No technique has so far exhibited this capability. Such a technique would also allow one to look at the tissue distribution of the agent in relation to tissue composition and explore whether the agent may highlight specific disease components. The aim of this study was to examine the capability of nuclear microscopy to map and quantify Gd in tissue sections.

There were three main objectives of this study. First, to determine whether or not nuclear microscopy is sufficiently sensitive to detect Gd in atherosclerotic aortic sections from cholesterol-fed rabbits after intravenous injection of bis-5-hydroxytryptamide-diethylenetriamine-pentaacetate gadolinium [bis-5HT-DTPA(Gd)]. Bis-5HT-DTPA(Gd) is an enzyme-activatable agent targeting myeloperoxidase (MPO) (Querol et al., 2005, 2006; Chen et al., 2006). MPO is an abundant heme enzyme released by activated leukocytes and catalyzes the formation of a number of reactive species that, among many harmful biological effects, can modify low-density lipoprotein to a form that converts macrophages into lipid-laden or "foam" cells, the hallmark of atherosclerotic lesions (Carr et al., 2000; Wada et al., 2000). Validation of this novel MPO-sensing imaging agent is an extremely important step toward the ultimate goal of producing magnetic resonance images that reflect atherosclerotic plaque vulnerability. For control, we sacrificed a cholesterol-fed rabbit 1 week after injection of the clinical standard agent diethylenetriamine-pentaacetate gadolinium [DTPA(Gd)]. This agent is the parent compound on which bis-5HT-DTPA(Gd) is based though it possesses no molecular specificity.

Second, we explored the use of this technique to detect changes in Gd levels over time by examining aortic sections obtained at 2 and 4 h after bis-5-HT-DTPA(Gd) injection. Third, high-resolution studies were also performed to evaluate if this particular agent had any preferential distribution within the aorta.

Materials and Methods

Animal Model and Sample Preparation

Aorta samples were obtained from three male New Zealand white rabbits fed on a low-level cholesterol diet. Two of the rabbits were fed on a diet of 0.25% w/w cholesterol diet for 8 months followed by 0.125% w/w cholesterol diet for another 10 months, while the third rabbit was fed the 0.25% diet for 17 months followed by the 0.125% diet for an additional year. This model was chosen because rabbits fed cholesterol-containing diet (0.15–0.3% w/w) over extended periods of time develop aortic lesions that resemble late stage human atherosclerotic lesions (Daley et al., 1994*a*, 1994*b*; Ronald et al., 2007). The first test rabbit (18 months on diet) received 0.2 mmol/kg of bis-5HT-DTPA(Gd) injection 2 h prior to sacrifice, while the second test rabbit (29 months on diet) received the injection 4 h prior to sacrifice. A third rabbit (18 months on diet) received DTPA(Gd) injection 1 week prior to the sacrifice. Previous nuclear microscopy experiments carried out at our center over the last decade have shown that once atherosclerosis sets in, the elemental distribution exhibits similar trends regardless of age or the duration of cholesterol feeding (Watt et al., 2006). These trends indicate that rabbits that have been fed a cholesterol diet for more than 1.5 years show significant lesion development (Ronald et al., 2007). Since the focus of the study was on assessing the capability of nuclear microscopy to measure Gd, the variations in age and duration of administration of the high cholesterol diet is unlikely to affect our ability to detect Gd. Animals were cared for in accordance with guidelines of the Canadian Council on Animal Care.

At sacrifice, each animal was sedated via an intramuscular injection of stock anesthetic [ketamine (23.4 mg/kg), xylazine (1.3 mg/kg), and glycopyrolate (0.02 mg/kg)]. Sedated animals were sacrificed with an intravenous injection of ketamine (200 mg) and transcardially-perfused under pressure with ∼1.5 L of heparinized (1 IU/mL) Hanks' balanced salt solution. Fresh-frozen aortic tissue blocks (5 mm thick) were collected every 3 mm superiorly, starting 1 cm above the celiac bifurcation. Three blocks were collected from the 2 h post rabbit and 4 blocks from the 4 h post rabbit. Cryostat sectioning was performed and two contiguous 10 μm sections from each block were collected on pioloform wrapped aluminum holders.

Mapping and Quantifying Gd: Nuclear Microscopy

Nuclear microscopy, using a combination of the three techniques—particle induced X-ray emission (PIXE), Rutherford backscattering spectroscopy (RBS), and scanning transmission ion microscopy (STIM)—has the unique capability to map multiple elements above sodium in the periodic table and simultaneously quantify them down to the ppm levels. Nuclear microscopy is ideally suited for measuring the trace elemental distributions in atherosclerotic tissue (Watt et al., 2006; Roijers et al., 2008).

The nuclear microscopy experiments were carried out at the Centre for Ion Beam Applications (CIBA) at the National University of Singapore (Watt et al., 2003). A 2.1 MeV proton beam was focused to a spot size of 1 μm and scanned across the region of interest. Data from the three techniques of STIM, PIXE, and RBS were simultaneously collected. STIM provides structural maps based on the energy lost by the protons as they pass through the relatively thin organic samples with thicknesses of 30 μm or less. This enables structural identification *without fixing or staining*. The trace elemental mapping was carried out by PIXE (Johansson et al., 1995), a nondestructive technique, which simultaneously detects multiple elements with high quantitative accuracy and with a sensitivity of down to 1 ppm in biological material such as tissue sections and

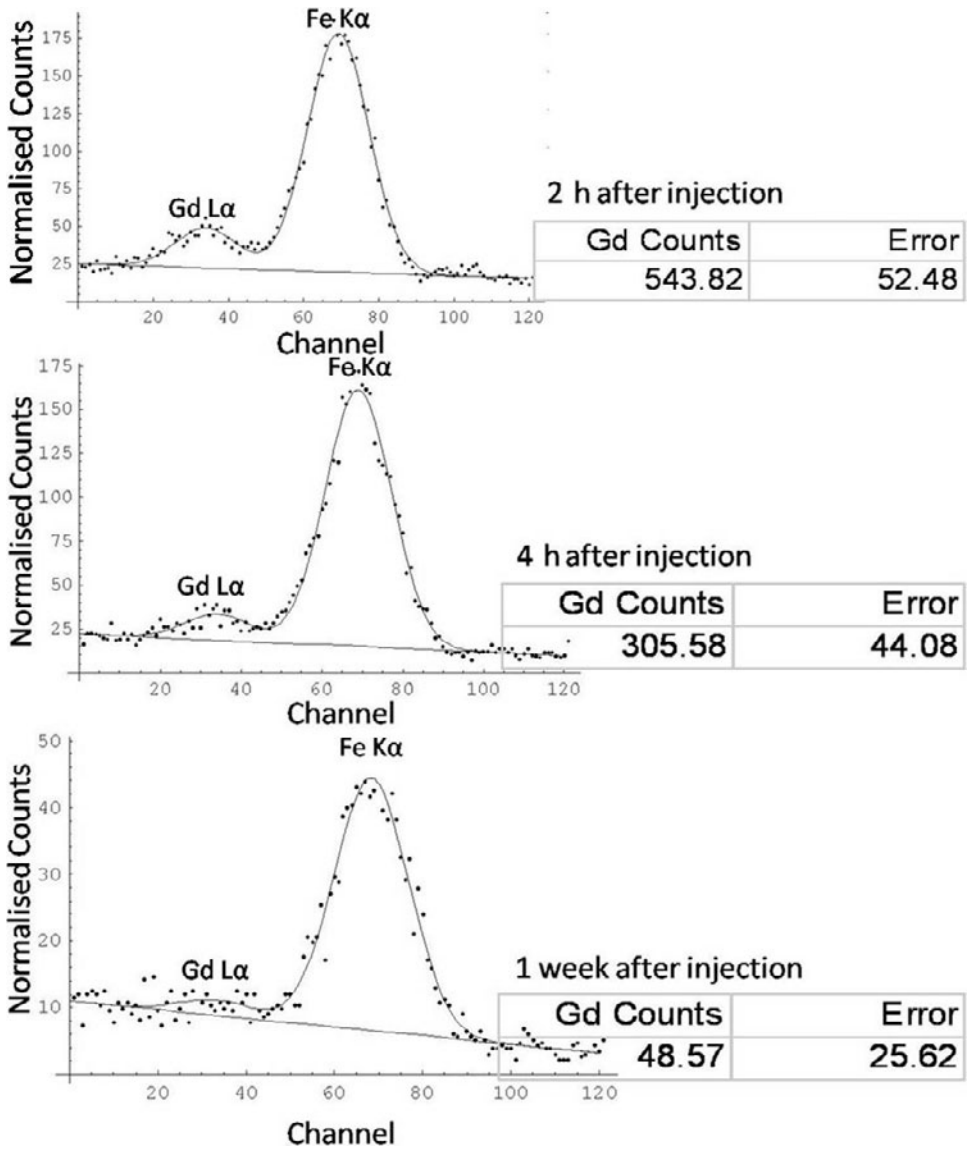

Figure 1. Mathematica fits of the 2- and 4-h samples show well-resolved Gd and Fe peaks and the comparative concentrations of gadolinium above the background level for the 2 and 4-h samples. The counts have been normalized to proton dose and tissue area. The control's (1-week) Gd peak is not as well resolved, consistent with being at the detection limit.

cells. The quantification in PIXE was validated by the use of a standard target of known elemental composition with certified homogeneity, manufactured by the National Institute of Standards and Technology (Gaithersburg, MD, USA). RBS was used to measure the concentration of matrix constituents of the sample. Large scans of 4 mm scan size were carried out to observe the overall distribution of the elements. To examine the spatial distribution of Gd, higher resolution scans were carried out (680 μm scan size) later. The data analysis was carried out using a combination of computer codes: SIMNRA (Mayer, 1997), Dan32, Gupix (Maxwell et al., 1989), and Mathematica.

Results and Discussion

Elemental Mapping: Gadolinium

Using the three techniques mentioned above, large area scans of 4 mm scan size were carried out to examine the overall distribution of the elements across the artery and lesion. To map gadolinium, the tissue was scanned by a 2.1 MeV proton beam. The collision of the beam with the atomic electrons in the sample and subsequent de-excitation leads to the emission of X-rays, which are unique to the parent atom. X-rays of different elements were detected

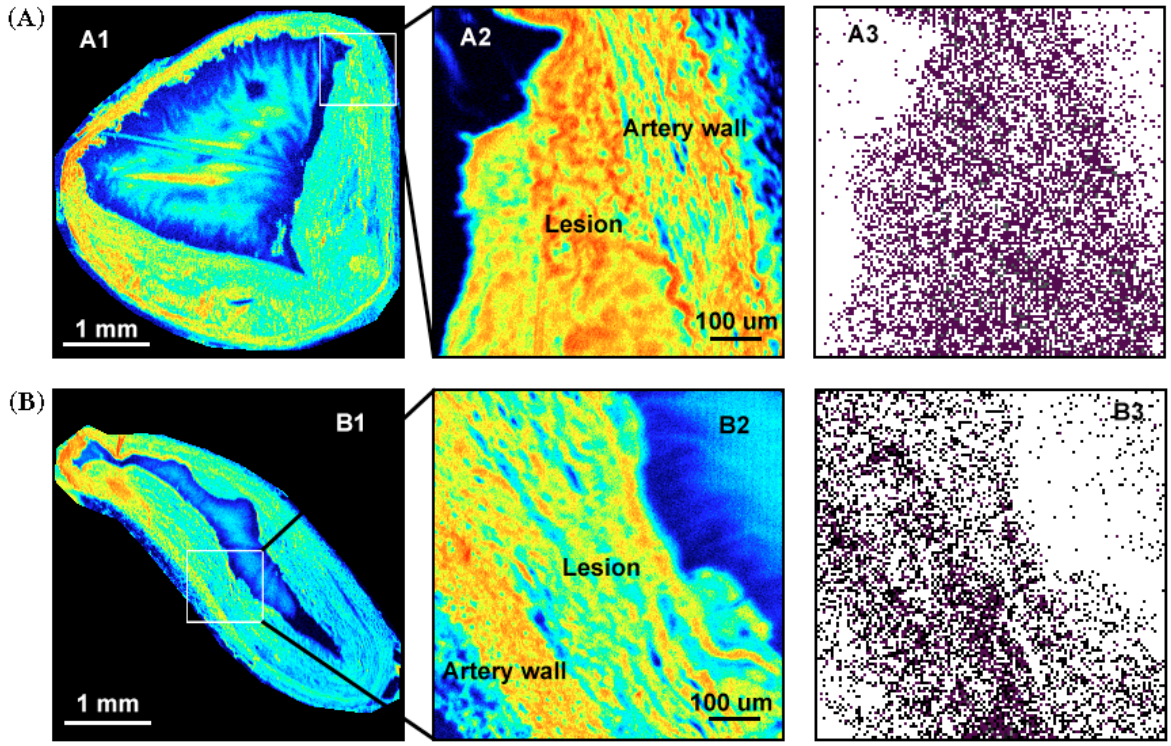

Figure 2. **A:** Overall STIM image of the 2-h rabbit section (A1), the corresponding high-resolution STIM image (A2) and Gd map (A3) obtained from the area depicted by the box in A1. **B:** Overall STIM image of the 4-h rabbit section (B1), the corresponding high-resolution STIM image (B2) and Gd map (B3) obtained from the area depicted by the box in B1.

simultaneously using a lithium-drifted silicon X-ray detector placed at 90° to the beam axis and fitted with a filter designed for detection of elements above sodium in the periodic table. Gadolinium was measured based on the emission of Gd Lα X-rays at energy of 6.05 keV. The well-resolved Mathematica fits of the PIXE spectrum with the Gd peak adjacent to the Fe Kα peak of one sample from each of the groups under study are shown in Figure 1. Our nuclear microscopy studies are the first to map gadolinium in unstained tissue.

To further describe the distribution of gadolinium throughout the diseased aortic wall, high-resolution studies were carried out. Areas comprising the atherosclerotic lesion and the adjacent artery walls were chosen for high-resolution nuclear microscopy scans. We obtained the tissue samples at fixed locations along the aorta. When we compared the Gd concentrations, no correspondence between the animals at the fixed locations was observed. In addition, no trend was identified within the same rabbit based on location along the aorta. The structural STIM maps and the gadolinium maps of the areas chosen for high-resolution studies are shown in Figure 2. The high-resolution studies showed that the gadolinium was relatively uniformly distributed across the tissue, without substantial preferential distribution, at both time points. Given that the agent has been demonstrated to be highly specific for MPO (Breckwoldt et al., 2008; Nahrendorf et al., 2008), we had hoped that we could detect a differential distribution pattern. However, as the tissue samples were collected several hours after bis-5HT-DTPA(Gd) administration (2 and 4 h post injection), it is not completely unexpected that Gd would be homogeneously distributed throughout the plaque as the agent is a small molecule and can diffuse easily throughout the tissues. Furthermore, this agent does not bind to MPO, but is activated by MPO to become oligomers with slower rotational dynamics to result in higher MRI signal intensity. Future studies will look at collecting tissue early after administration of the agent (within the first 30 min) where preferential distribution within the fibrous cap of the plaques has been described (Wasserman et al., 2005). Alternatively, an agent known to distribute inhomogenously within atherosclerotic tissue such as Gadofluorine-M (Meding et al., 2007) could be used.

Quantitative Analysis: Gadolinium

To calculate the elemental concentrations, the data obtained from PIXE and RBS were analyzed using a combination of various computer codes: SIMNRA, Dan 32, Gupix, and Mathematica. To eliminate the possibility of errors in the

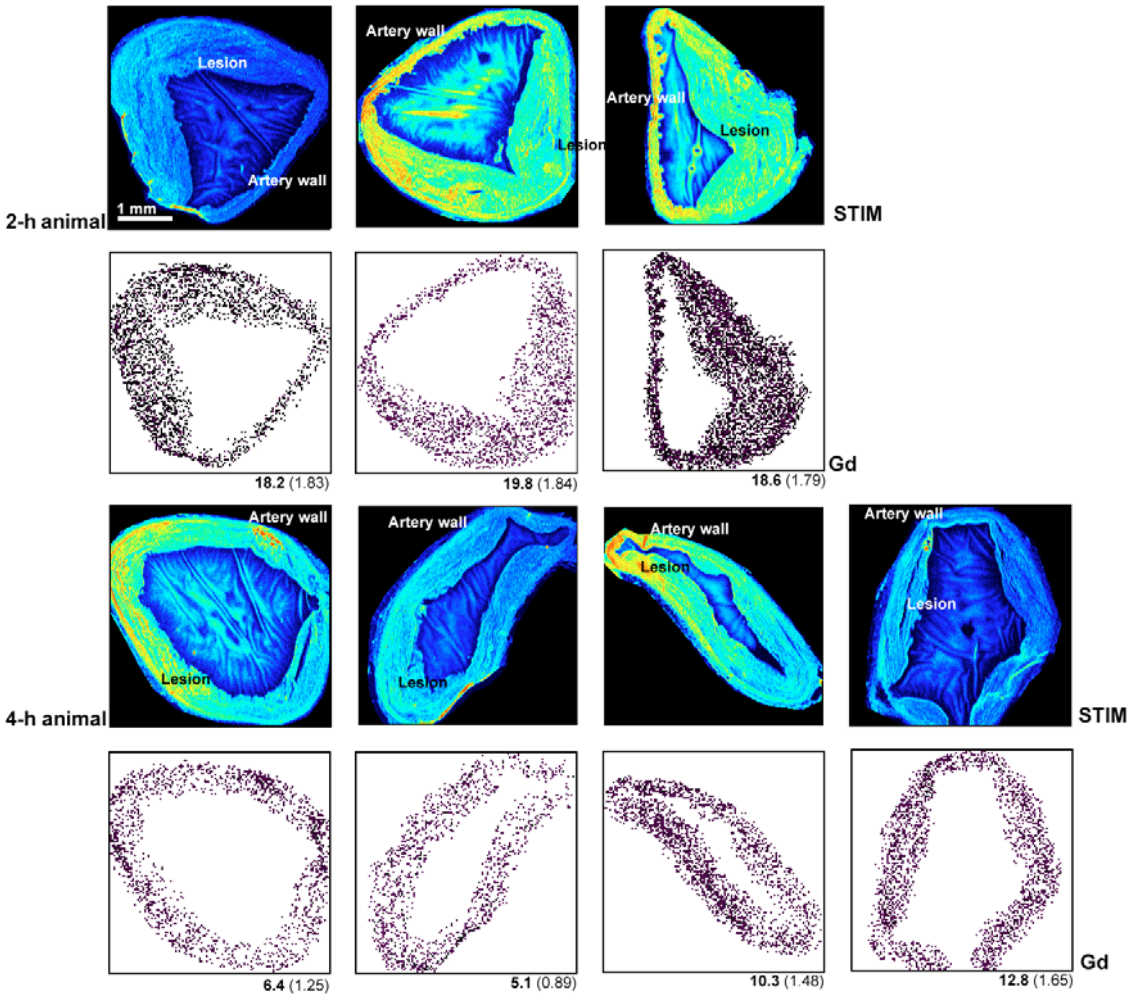

Figure 3. STIM and the corresponding PIXE maps comparing the gadolinium distribution and concentration in the 2- and 4-h animals of the sections at fixed locations along the aorta. The Gd concentration in ppm is shown below each map with the errors in brackets.

counts of the Gd Lα peak (6.056 keV) due to the proximity of the large number of counts of the adjacent Fe kα peak (6.398 keV), the Gd peak from each PIXE spectra was manually fitted using Mathematica and the area counts (minus the background) and percentage errors obtained. These results, in conjuction with Gupix, helped to determine the concentration at the ppm level. The Gd and the Fe peaks are seen sufficiently resolved in the Mathematica fits of the PIXE spectrum (Fig. 1).

Our studies showed that the gadolinium concentration was below 20 ppm in all the sections examined. This cannot be compared to any previously known figures for verification as Gd has never been quantified in this manner before. Figure 3 compares the overall distribution and concentration of Gd in the 4-h group to that in the 2-h group of the sections at fixed locations along the aorta. The average concentrations of Gd are shown in the graph (Fig. 4). The

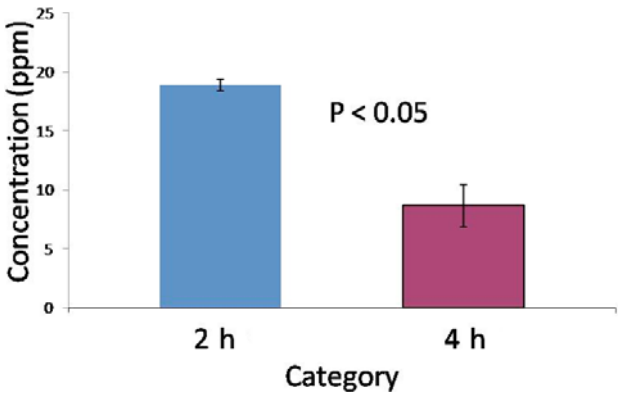

Figure 4. The average concentration of gadolinium in the 2- and 4-h samples. A significant difference was observed between the concentrations of the 2- and 4-h samples. Error bars depict the standard errors of the averages.

Gd concentration is consistently higher for the 2-h group compared to the 4-h group, with the averages showing a significant difference ($p < 0.05$) The 4-h group also showed a greater variation in concentration (standard deviation = 3.5 ppm) compared to the 2-h group (standard deviation = 0.8 ppm).

The clearance of Gd in humans depends on various factors including the compound used (Bremerich et al., 2001), the tissue type, and the age of the patients (Baker et al., 2004). While the number of animals used in this proof-of-principle study is small, it would be useful to compute a clearance rate as an example of the type of analysis that can be obtained from the technique we developed in this study. For bis-5HT-DTPA(Gd) in diseased aortic wall from rabbits, the clearance time for Gd concentration to drop by a factor of 2 in this study was 1.64 h. This was obtained by fitting the data points corresponding to the measured concentration at 2 and 4 h to an exponential decay model. While the small samples size used in this study precludes definitive conclusions to be made from this calculation, this value is nonetheless similar to the biological elimination half-life of 1.5 h calculated for human patients (Bellin, 2006).

The tissues obtained at 1 week after DTPA(Gd) injection was used as a control as at this time point the agent would be cleared from the tissues. Indeed, the Gd concentration we obtained was dramatically lower than at 2 and 4 h (2 h = 18.86 ppm, 4 h = 8.65 ppm). The Gd concentrations for the 1 week sample (2.7 ppm) is at the detection threshold of the PIXE technique, estimated to be about 2–3 ppm for Gd and therefore not significant. A comparison of the Mathematica fits of the 2-h, 4-h, and 1-week animals illustrates this (Fig. 1).

Conclusion

Nuclear microscopy has, for the first time, simultaneously mapped and quantified Gd in tissue sections obtained after intravenous administration of a Gd-based MR CA. The techniques described here can be used to image Gd-based compounds, and we believe they will be particularly applicable for assessing optically-silent conventional and novel MRI agents. Furthermore, the quantitative nature of our technique was sufficiently sensitive to changes in Gd concentration over time. Comparing the Gd concentration in the arteries of rabbits sacrificed 2 and 4 h after intravenous injection of gadolinium agents, it was found that the concentration of Gd was consistently higher in the 2-h animal compared to the 4-h animal. The 1-week control did not show any significant residual gadolinium in the tissue.

This study illustrates the possibility of using nuclear microscopy to better understand the mechanism of Gd-based MRI agents and to map and quantify the biodistribution of these agents at very high spatial resolution. Our findings suggest that nuclear microscopy could be developed as a quantitative standard to complement MRI, in animal or human studies where tissues may be removed after imaging. In the future, by comparing the nuclear microscopy maps to adjacent histological sections, we can further understand the biodistribution of Gd-chelates that localize to specific structures that may be revelant to disease characterization and/or progression.

Acknowledgments

We thank Kem Rogers, Amanda Hamilton, Elisenda Rodriguez, Andre Belisle, Gloria Chiang, Allison Lee, and Fred Reynolds for experimental assistance. We also acknowledge early contributions by Alexei Bogdanov and Manel Querol in developing bis-5HT-DTPA(Gd). B.K.R. holds the Barnett-Ivey Heart and Stroke Foundation of Ontario Research Chair. J.A.R. holds the Great-West Life doctoral research award from the Heart and Stroke Foundation of Canada. The work was supported in part by the National Institute of Health grants KO8HL081170 (J.W.C.) and RO1-HL078641 (R.W., B.K.R.).

References

Baker, J.F., Kratz, L.C., Stevens, G.R. & Wible, J.H., Jr. (2004). Pharmacokinetics and safety of the MRI contrast agent gadoversetamide injection (OptiMARK) in healthy pediatric subjects. *Invest Radiol* **39**(6), 334–339.

Bellin, M.F. (2006). MR contrast agents, the old and the new. *Eur J Radiol* **60**, 314–323.

Brasch, R.C. (1992). New directions in the development of MR imaging contrast media. *Radiology* **183**, 1–111.

Breckwoldt, M.O., Chen, J.W., Stangenberg, L., Aikawa, E., Rodriguez, E., Qiu, S., Moskowitz, M.A. & Weissleder, R. (2008). Tracking the inflammatory response in stroke *in vivo* by sensing the enzyme myeloperoxidase. *Proc Natl Acad Sci USA* **105**(47), 18584–18589.

Bremerich, J., Colet, J.M., Giovenzana, G.B., Aime, S., Schefler, K., Laurent, S., Bongartz, G. & Muller, R.N. (2001). Slow clearance gadolinium-based extracellular and intravascular contrast media for three-dimensional MR angiography. *J Magn Reson Imaging* **13**(4), 588–93.

Carr, A.C., Myzak, M.C., Stocker, R., McCall, M.R. & Frei, B. (2000). Myeloperoxidase binds to low-density lipoprotein: Potential implications for atherosclerosis. *FEBS Lett* **487**(2), 176–180.

Chen, J.W., Sans, M.Q., Bogdanov, A. & Weissleder, R. (2006). Imaging of myeloperoxidase in mice by using novel amplifiable paramagnetic substrates. *Radiol* **240–242**, 473–481.

Daley, S.J., Herderick, E.E., Cornhill, J.F. & Rogers, K.A. (1994*a*). Cholesterol-fed and casein-fed rabbit models of atherosclerosis. Part 1: Differing lesion area and volume despite equal plasma cholesterol levels. *Arterioscler Thromb* **14**(1), 95–104.

Daley, S.J., Klemp, K.F., Guyton, J.R. & Rogers, K.A. (1994*b*). Cholesterol-fed and casein-fed rabbit models of atherosclerosis. Part 2: Differing morphological severity of atherogenesis despite matched plasma cholesterol levels. *Arterioscler Thromb* **14**(**1**), 105–141.

Idee, J-M., Port, M., Raynal, I., Schaefer, M., Greneur, S.L. & Corot, C. (2006). Clinical and biological consequences of transmetallation induced by contrast agents for magnetic resonance imaging: A review. *Fundam Clin Pharmacol* **20**, 563–576.

Johansson, S.A.E., Campbell, J.L. & Malmqvist, K.G. (1995). *Particle Induced X-Ray Emission Spectrometry (PIXE)*. Chichester, U.K.: John Wiley & Sons.

Maxwell, J.A., Campbell, J.L. & Tesdale, W.J. (1989). The Guelph PIXE software package. *Nucl. Instrum Methods B* **43**, 218.

Mayer, M. (1997). *Simnra Users' Guide*. Technical Report IPP 9/113, Max-Planck Institut for Plasmaphysik, Garching, Germany.

Meding, J., Urich, M., Licha, K., Reinhardt, M., Misselwitz, B., Fayad, Z.A. & Weinmann, H.J. (2007). Magnetic resonance imaging of atherosclerosis by targeting extracellular matrix deposition with Gadofluorine M. *Contast Media Mol Imag* **2**(3), 120–129.

Nahrendorf, M., Sosnovik, D., Chen, J.W., Panizzi, P., Figueiredo, J.L., Aikawa, E., Libby, P., Swirski, F.K. & Weissleder, R. (2008). Activatable magnetic resonance imaging agent reports myeloperoxidase activity in healing infarcts and noninvasively detects the antiinflammatory effects of atorvastatin on ischemia-reperfusion injury. *Circulation* **117**(9), 1153–1160.

Querol, M., Chen, J.W. & Bogdanov, A.A., Jr. (2006). A paramagnetic contrast agent with myeloperoxidase-sensing properties. *Org Biomol Chem* **4**(10), 1887–1895.

Querol, M., Chen, J.W., Weissleder, R. & Bogdanov, A., Jr. (2005). DTPA-bisamide-based MR sensor agents for peroxidase imaging. *Org Lett* **7**(9), 1719–1722.

Roijers, R.B., Dutta, R.K., Cleutjens, J.P.M., Mutsaers, P.H.A., de Goeij, J.J.M. & van der Vusse, G.J. (2008). Early calcifications in human coronary arteries as determined with a proton microprobe. *Anal Chem* **80**(1), 55–61.

Ronald, J.A., Walcarius, R., Robinson, J.F., Hegele, R.A., Rutt, B.K. & Rogers, K.A. (2007). MRI of early and late-stage arterial remodeling in a low level cholesterol-fed rabbit model of atherosclerosis. *J Magn Reson Imaging* **26**, 1010–1019.

Strijkers, G.J., Mulder, J.M.W., Van Tilborg, G.A.F. & Nicolay, K. (2007). MRI contrast agents: Current status and future perspectives. *Anti-Cancer Agents Med Chem* **7**, 291–305.

Wada, Y., Sugiyama, A., Kohro, T., Kobayashi, M., Takeya, M., Naito, M. & Kodama, T. (2000). *In vitro* model of atherosclerosis using coculture of arterial wall cells and macrophage. *Yonsei Med J* **41**(6), 740–755.

Wasserman, B.A., Casal, C.S., Astor, B.C., Aletras, A.H. & Arai, A.E. (2005). Wash-in kinetics for gadolinium-enhanced magnetic resonance imaging of carotid atheroma. *J Magn Reson Imaging* **21**(1), 91–95.

Watt, F., Rajendran, R., Ren, M.Q., Tan, B.K.H. & Halliwell, B. (2006). A nuclear microscopy study of trace elements Ca, Fe, Zn and Cu in atherosclerosis. *Nucl Instrum Methods Phys Res B* **249**, 646–652.

Watt, F., Van Kan, J.A., Rajta, I., Bettiol, A.A., Choo, T.F., Breese, M.B.H. & Osipowicz, T. (2003). The National University of Singapore high energy ion nano-probe facility: Performance tests. *Nucl Instrum Methods Phys Res B* **210**, 14–20.